2013

CFD Simulation of Different-Scaled Bubbling Fluidized Beds

Jungkee Jang
Illinois Institute of Technology, USA

Hamid Arastoopour
Illinois Institute of Technology, USA

CFD SIMULATION OF DIFFERENT-SCALED BUBBLING FLUIDIZED BEDS

Jungkee Jang and Hamid Arastoopour
Illinois Institute of Technology
Perlstein Hall, 10 W. 33rd Street
Chicago, IL 60616

ABSTRACT

A reliable design and scale-up approach for a bubbling fluidized bed process requires a very detailed model based on the fundamentals of multiphase transport phenomena. The present study addresses the simulation and scale-up of rather complex gas-solid flow behavior in bubbling beds using a Computational Fluid Dynamics (CFD) approach and 3-Dimensional Simulation.

INTRODUCTION

In the literature, there are extensive studies on gas-solid flow systems in bubbling fluidized beds. However, achieving a fundamental understanding of the mechanisms governing the behavior of the bubbling fluidized beds, particularly under industrial operating conditions, still presents a major scientific and engineering challenge [1,2]. The reliable design of commercial-scale plants requires not only a comprehensive understanding of the complex flow phenomena in the bubbling fluidized beds, but also a detailed knowledge of how hydrodynamics are affected by both geometry and scale-up [3].

In the present study, 3-Dimensional (3-D) simulations of bubbling beds for both the PSRI/NETL laboratory and large-scale fluidized beds using the kinetic theory approach were performed. First, *our* CFD *model* was validated by comparing the results with the laboratory-scale experimental data of PSRI/NETL, then was refined by selecting proper drag force expression and boundary condition prameters. Our refined 3-D CFD model was used to predict the large-*scale PSRI bubbling* fluidized bed performance. Our numerical simulation results compared well with both PSRI large-scale experimental data on time-averaged pressure drop and void fraction.

CFD MODEL

The CFD model used in this study is based on the Eulerian-Eulerian approach two-fluid granular model (TFM). The kinetic theory of granular flows was used to describe the particulate phase flow behavior in our bubbling fluidized bed and to develop a constitutive relation to close our governing equations. A set of governing equations (continuity, momentum, and granular temperature) to describe the hydrodynamics of the gas-solid flow in a bubbling fluidized bed was

solved using a commercial CFD code, ANSYS/FLUENT 13. Tables 1 and 2 show the continuity, momentum, granular temperature, and all constitutive equations used for the closure of the governing equations [4,5,6]. In order to describe the frictional force between particles for the case of solid volume fraction higher than frictional packing limit ($\varepsilon_s > \varepsilon_{fr} = 0.56$), the frictional stress term was considered as a major stress tensor and the corresponding frictional pressure and viscosity were also used (see Table 2). Our calculated pressure drop versus gas velocity agreed well with laboratory scale PSRI/NETL experimental data using Syamlal-O'Brien drag force expression [7]. Therefore, Syamlal-O'Brien drag force expression was also used to simulate PSRI/NETL large scale experiments.

NUMERICAL METHOD AND BOUNDARY CONDITIONS

To simulate the actual PSRI/NETL laboratory-scale and large-scale bubbling fluidized bed processes and to accurately predict the gas-solid flow patterns, a 3-D geometry system was considered. After performing the grid-independent tests, 10,796 and 120,181 computational meshes were chosen for lab-scale and large-scale bubbling beds, respectively. These mesh numbers are the minimum mesh numbers needed to obtain grid-independent results [5]. For the large scale experiments, unstructured meshes with minumum size of 0.15 cm and maximun size of 1.5 cm (for the bed region) and minimun size of 3.5 cm and maximum size of 7.0 cm (for the free board regin) were Used. The governing and constitutive equations were solved using a pressure-based solution algorithm. To avoid solution divergence, small time steps on the order of 1×10^{-4} were adopted. Convergence was set to occur when the scaled residuals reported for all variables fell below 1×10^{-4}. The computationl time for a typical large scale simulation run was about two weeks using CPU 3.3 GHZ.

Initially, the gas velocity was set to be zero throughout the entire bed. The velocity profile for the gas phase was applied as an inlet condition. A value for the pressure was specified at the outlet of the fluidized bed. For the gas phase, no-slip and non-penetrating wall conditions were used as the wall boundary condition. For the solid phase, the Johnson and Jackson boundary condition [6] was used as the wall boundary condition with particle-wall restitution coefficient of 0.2 and specularity coefficient of 0.3. The particle-particle restitution coefficient of 0.9 was used in all of our simulations. Table 3 shows the simulation input and parameters which are the same as the conditions used in the PSRI/NETL experiments.

DESCRIPTION OF PSRI / NETL EXPERIMENT

The PSRI/NETL laboratory bubbling fluidized bed (0.15 m diameter and 1.83 m height) was used in the minimum fluidization experiment (small-scale experiment). Fluid Catalytic Cracking (FCC) particles with 3% fines (less than 44 μm) were used as bed materials. The weight of a particle batch was 6.8 kg, and the particle density was 1,489 kg/m^3.

In the PSRI/NETL large-scale bubbling fluidized bed (0.9 m diameter and 6.1 m height) experiments, FCC particles with 12% fines were used as the bed material. Figure 1 shows the schematic of an air distributor having 39 small jets with a 30 degree angle from vertical used in this experiment. In this experiment, time-averaged pressure drop as a function of the height (z-direction) and void

fraction at different radial locations (r-direction) at a bed height of 1.52 m were measured [8]. The particles used are Geldart Type A particles.

RESULTS AND DISCUSSION

To predict the characteristics of gas-solid flow patterns in the PSRI/NETL laboratory-scale minumun fluidization experiment and the large-scale bubbling fluidized bed, exactly the same bed dimensions and inlet configurations (such as air distributor) as those in the experiments were used in our 3-D simulations. First, we performed the simulation of the PSRI laboratory-scale fluidized bed before attempting the simulation of a PSRI large-scale bubbling bed to validate, and refine our CFD model for a large-scale simulation. Based on our refined

CFD model, we performed the simulation of the large-scale bubbling fluidized bed. Table 3 shows the simulation inputs and parameters, which are the same as those used by the PSRI/NETL experiments.

Figure 2 shows a comparison of our simulation results with PSRI/NETL experimental data at the laboratory-scale bubbling fluidized bed after minimum fluidization velocity and before bubbling velocity. The simulation and experimental results describe a pressure drop at a height between 0.39 m and 0.24 m (differential pressure drop across 0.15 m) as a function of superficial inlet air velocity using FCC particles with 3% fines. The superficial gas velocity of 0.0021 m/s was measured as the minimum fluidization velocity. In order to predict the pressure drop in the PSRI/NETL laboratory-scale fluidized bed, we carried out a 3-D simulation with particles of 73 μm average size using different superficial gas velocities of 0.0021 m/s, 0.006 m/s, 0.01 m/s, and 0.014 m/s, respectively. According to Figure 2, our simulation result shows a very good agreement with the PSR/NETLI experimental data for pressure drop versus superficial gas velocity between minimum fluidization and minimum bubbling regimes. A small deviation of our simulation from experimental data at a superficial gas velocity of 0.006 m/s could be due to the slight cohesivity of the Group A particles used in the experiments. In our CFD model, we considered only frictional forces and cohesive forces were not included in our model. Overall, our simulation result predicts well the pressure drop at minimum fluidization velocity in comparison to the experiment data. Based on our simulation of the laboratory-scale fluidized bed, assumptions such as uniform particle size, 3-D geometry, boundary conditions, and drag coefficient are reasonable and are used in the simulation of a PSRI/NETL large-scale fluidized bed.

Figure 3 shows the PSRI/NETL large-scale simulation of the solid volumetric concentration (X-Z plane view) at different times (10 s, 20 s, and 30 s). According to this figure, no bubbles were formed. The bed height was expanded considerably with approximately uniform particle distribution throughout the bed. In our simulations, similar to the experiment, an air distributor having 39 small jets with a 30 degree angle was considered. The small jets at a 30 degree angle broke the bubbles, so that large bubbles with higher void fraction were not observed in our simulation, which is in line with the experimental data and observations.

Figure 4 shows the comparison of our pressure drop simulation result with PSRI/NETL large-scale experimental data. FCC particles with 12% fines were used as bed materials. The static bed height and inlet superficial gas velocity were 2.44 m and 0.6 m/s, repectively. Figure 4 shows our 3-D simulation result

on the pressure drop along the bed agreed well with the experimental data. The time-averaged pressure drop (50-150 s) calculated values show the pressure drop significantly decreased at a height of around 3 m similar to the experimental data. Our 3-D simulation accurately predicted the bed height expansion.

Figure 5 shows time-averaged (50-150 s) bubbling void fraction at different radial locations at a bed height of 1.52 m. Our simulation result is in very good agreement with the PSRI/NETL large-scale experimental data. According to this figure, the solid void fraction is not symmetric with respect to the center of the bed. Similar to the experimental data, our simulation showed that the higher void fraction regions occurred at the center of the bed.

CONCLUSION

Our 3-D model and simulation described well the gas-solid flow patterns of the PSRI/NETL small- and large-scale bubbling fluidized beds. Our 3-D model which incorporates the exact experimental air distributor design as input to our simulation is very successful in predicting the important gas-solid hydrodynamics such as mixing, pressure drop, solid void fraction distribution inside the bed, and bed height expansion. The comparisons between our simulation of pressure drop at different positions and solid void fraction with the experimental data at two different scales showed the excellent capability of our CFD-based multiphase model and simulation as a tool in the design and scale-up of the processes based on bubbling fluidized beds.

NOTATION

		Greek	
C_D	Drag function	τ	Stress tensor, Pa
e_{ss}	Restitution coefficient	ε	Volume fraction
g	Gravity, m/s^2	μ	Viscosity, Pa·s
I_{2D}	Second invariant of deviatonic tensor		
$\bar{I}$	Identity tensor	θ	Granular temperature, m^2/s^2
k_{θ_s}	Granular conductivity	ρ	Density, Kg/m^3
k_{g_s}	Granular energy exchange coefficient	ϕ	Angle of internal friction
K_{sg}	Drag coefficient		
p	Pressure, Pa	*Subscript*	
		s	Solid phase
		g	Gas phase
$\vec{v}$	Velocity, m/s	*fr*	Friction

REFERENCES

[1] J. K. Jang, C. Roza, and H. Arastoopour, "CFD Simulation of Pharmaceutical Particle Drying in a Bubbling Fluidized Bed Reactor," in *Fluidization XIII*, pp. 853-860, 2010.

[2] H. Arastoopour, "Numerical Simulation and Experimental Analysis of Gas/Solid Flow Systems: 1999 Fluor-Daniel Plenary Lecture," *Powder Technology Journal,* Vol. 119, pp. 59-67, Sept. 24, 2001.

[3] F. Taghipour, N. Ellis, and C. Wong, "Experimental and Computational Study of Gas-Solid Fluidized Bed Hydrodynamics," *Chemical Engineering Science,* Vol. 60, pp. 6857-6867, Dec. 2005.

[4] D. Gidaspow, *Multiphase Flow and Fluidization: Continuum and Kinetic Theory Descriptions*. Boston: Academic Press, 1994.

[5] J. Jang, "Modeling and Computational Fluid Dynamics Simulation of a Bubbling Fluidized Bed Process at Different Scale," Ph.D. thesis Illinois Institute of Technology, 2012.

[6] P. C. Johnson and R. Jackson, "Frictional Collisional Constitutive Relations for Antigranulocytes-Materials, with Application to Plane Shearing," *Journal of Fluid Mechanics*, Vol. 176, pp. 67-93, March 1987.

[7] M. Syamlal and T. J. O'Brien, "Computer Simulation of Bubbles in a Fluidized Bed," *AIChE Symposium Series,* Vol. 85, pp. 22-31, 1989.

[8] L. Shadle, M. Shahnam, C. Guenther, and R. Cocco, "NETL 2011 Workshop on Multiphase Flow Science," Pittsburgh, PA, Aug. 16 2011.

Table 1. Governing Equations for TFM Model

Continuity equation

Gas phase

$$\frac{\partial}{\partial t}(\varepsilon_g \rho_g) + \nabla \cdot (\varepsilon_g \rho_g \vec{v}_g) = 0$$

Solid phase

$$\frac{\partial}{\partial t}(\varepsilon_s \rho_s) + \nabla \cdot (\varepsilon_s \rho_s \vec{v}_s) = 0$$

Conservation of momentum

Gas phase

$$\frac{\partial(\varepsilon_g \rho_g \vec{v}_g)}{\partial t} + \nabla \cdot (\varepsilon_g \rho_g \vec{v}_g \vec{v}_g) = -\varepsilon_g \nabla p + \nabla \cdot \bar{\bar{\tau}}_g + \varepsilon_g \rho_g g + K_{gs}(\vec{v}_g - \vec{v}_s)$$

Solid phase

$$\frac{\partial(\varepsilon_s \rho_s \vec{v}_s)}{\partial t} + \nabla \cdot (\varepsilon_s \rho_s \vec{v}_s \vec{v}_s) = -\varepsilon_s \nabla p + \nabla \cdot \bar{\bar{\tau}}_s + \varepsilon_s \rho_s g + K_{sg}(\vec{v}_s - \vec{v}_g)$$

Granular temperature equation

$$\frac{3}{2}[\frac{\partial}{\partial t}(\rho_s \varepsilon_s \theta_s) + \nabla \cdot (\rho_s \varepsilon_s \vec{v}_s \theta_s)] = (-p_s \bar{\bar{I}} + \bar{\bar{\tau}}_s) : \nabla \cdot \vec{v}_s + \nabla \cdot (k_{\theta_s} \nabla \theta_s) - \gamma \theta_s + \phi_{gs}$$

Table 2. Constitutive Relations for TFM Model

Stress tensor for gas phase

$$\tau_g = 2\varepsilon_g \mu_g \{\frac{1}{2}(\nabla v_g + \nabla v_g^T) - \frac{1}{3}(\nabla \cdot v_g)\bar{I}\}$$

Stress tensor for solid phase

$$\bar{\bar{\tau}}_s = (\varepsilon_s \mu_b \nabla \cdot \vec{v}_s)\bar{I} + 2\varepsilon_s \mu_s \{\frac{1}{2}(\nabla \vec{v}_s + \nabla \vec{v}_s^T) - \frac{1}{3}(\nabla \cdot \vec{v}_s)\bar{I}\}$$

Solid pressure

$$p_s = p_{kinetic} + p_{collision} = \varepsilon_s \rho_s \theta_s + 2\rho_s (1+e_{ss})\varepsilon_s^2 g_o \theta_s \qquad (\varepsilon_s < \varepsilon_{s,fr})$$

$$p_s = p_{kinetic} + p_{friction} = \varepsilon_s \rho_s \theta_s + Fr\frac{(\varepsilon_s - \varepsilon_{s,\min})^2}{(\varepsilon_{s,\max} - \varepsilon_s)^3} \quad where\ Fr = 0.1\varepsilon_s \quad (\varepsilon_s > \varepsilon_{s,fr})$$

Granular temperature conductivity

$$k_{\theta_s} = \frac{15 d_s \rho_s \varepsilon_s \sqrt{\theta_s \pi}}{4(41-33\eta)}[1+\frac{12}{5}\eta^2(4\eta-3)\varepsilon_s g_o + \frac{16}{15\pi}(41-33\eta)\eta\varepsilon_s g_o)], \quad where\ \eta = 0.5(1+e_{ss})$$

Solid viscosity

$$\mu_b = \frac{4}{3_s}\varepsilon_s \rho_s d_s g_o (1+e_{ss})(\frac{\theta_s}{\pi})^{1/2}$$

$$\mu_s = \mu_{s,col} + \mu_{s,kin} + \mu_{s,fr}$$

$$\mu_{s,kin+col} = \frac{\varepsilon_s \rho_s d_s \sqrt{\theta_s \pi}}{6(3-e_{ss})}[1+\frac{2}{5}(1+e_{ss})(3e_{ss}-1)\varepsilon_s g_o]$$

$$\mu_{s,col} = \frac{4}{5}\varepsilon_s \rho_s d_s g_o (1+e_{ss})(\frac{\theta_s}{\pi})^{1/2}$$

$$\mu_{s,kin+fr} = \frac{p_s \sin\phi}{2\sqrt{I_{2D}}}$$

Radial distribution

$$g_o = [1-(\frac{\varepsilon_s}{\varepsilon_{s,\max}})^{\frac{1}{3}}]^{-1}$$

Dissipation of granular energy

$$\gamma_{\theta_s} = \frac{12(1-e_{ss}^2)g_0}{d_s\sqrt{\pi}}\rho_s \varepsilon_s^2 \theta_s^{3/2}$$

Granular energy exchange between phases

$$\phi_{gs} = -3k_{gs}\theta_s$$

Table 3. Simulation Inputs and Parameters

	Lab-scale	Large-scale
Average particle size, μm	73	65
Initial bed height, m	0.457	2.44
Inlet gas velocity, m/s	0.0021, 0.006, 0.01, 0.014	Vz = 0.46 Vr = 0.26
Initial solid volume fraction	0.54	0.54

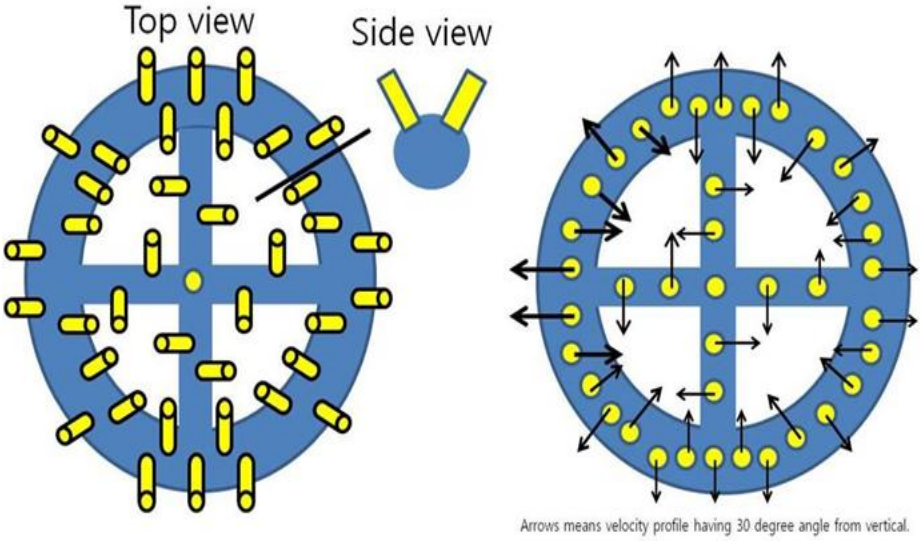

Figure 1. 3-D Views PSRI/NETL Ring Sparger Type Air Distributor

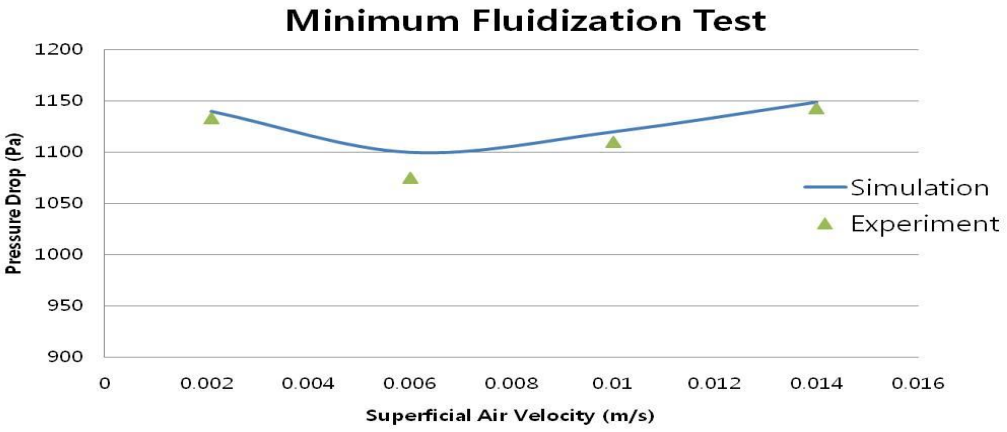

Figure 2. Comparison Between Our Simulation Results and PSRI/NETL Lab-scale Experimental Data

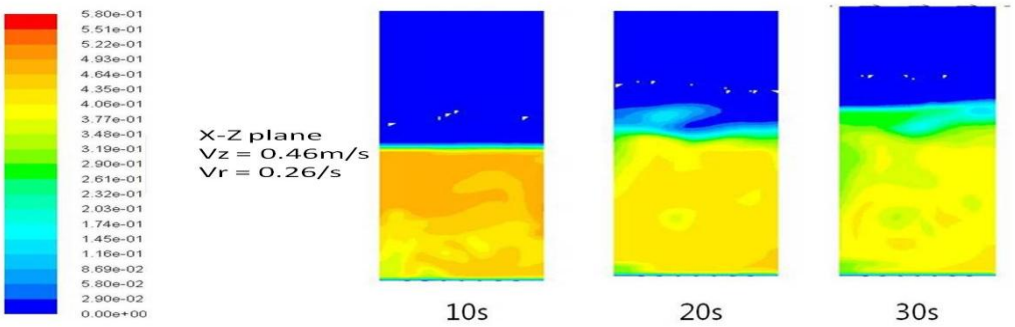

Figure 3. 3-D Simulation of Solid Volumetric Concentration (X-Z plane view) of PSRI/NETL Large-scale Fludized Bed at Different Times

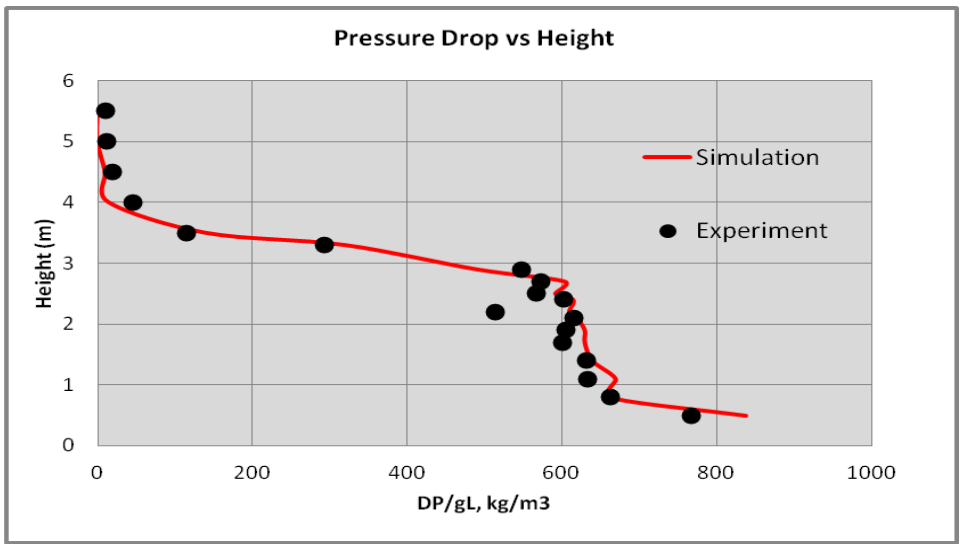

Figure 4. Comparison of Pressure Drop along the Bed Height between Our 3-D Simulation and the PSRI/NETL Large-scale Fluidized Bed Experiment

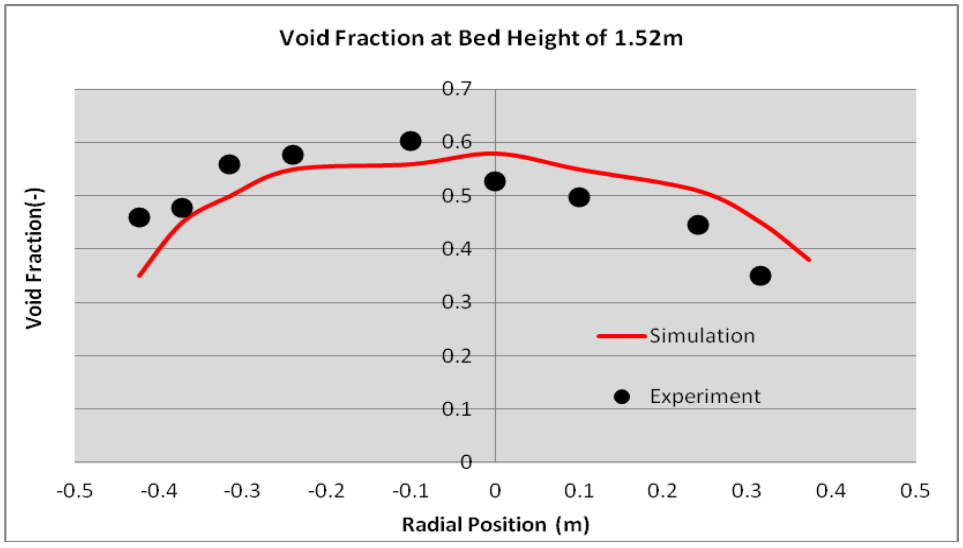

Figure 5. Comparison of Void Fraction at Different Radial Positions between Our 3-D Simulation and the PSRI/NETL Large-scale Fluidized Bed Experimental Data